Effect of Printing Parameters on Mechanical Properties, Warpage of 3D Printed PEEK/CF-PEEKComposites Using Multi-Objective Optimization Technique

Adarsh Sorekunte Huchappa and Nagamadhu Mahadevappa *

Posted Date: 21 April 2025

doi: 10.20944/preprints202504.1706.v1

Keywords: Additive Manufacturing (AM); Poly-Ether-Ether-Ketone (PEEK); Fused Dep-osition Modeling (FDM); Warpage; ANOVA; MOOM

 doi:10.20944/preprints202504.1706.v1

Article

Effect of Printing Parameters on Mechanical Properties, Warpage of 3D Printed PEEK/CF-PEEK composites Using Multi-Objective Optimization Technique

Adarsh S H [1] and Nagamadhu M [2,*]

[1] Department of Mechanical Engineering, Siddaganga Institute of Technology, Tumkur, Karnataka, India; adi1985nitk@gmail.com https://orcid.org/0000-0002-3620-5089

[2] Department of Mechanical Engineering, BMS Institute of Technology and Management, Bangalore, Karnataka, India, nagamadhu74@gmail.com and nagamadhum@bmsit.in.

* Correspondence: nagamadhu74@gmail.com

Abstract: Polyether Ether Ketone (PEEK) is a high-performance thermoplastic widely used in aerospace, automotive, and medical applications due to its exceptional strength, heat resistance, and chemical stability. However, warpage and mechanical property variations remain significant challenges in 3D printing PEEK parts. This study investigates the effect of key printing parameters, including nozzle temperature, layer thickness, platform temperature, and infill rate, on the mechanical properties and warpage of 3D-printed PEEK components. By systematically analyzing tensile and compressive loading conditions, this research aims to optimize printing settings to improve dimensional accuracy and structural integrity. Experimental results indicate that mechanical properties, such as tensile and compressive stress at break, vary significantly with printing conditions. The highest tensile strength of 71.4 MPa and compressive strength of 167 MPa were achieve. Meanwhile, lower tensile (45.36 MPa) and compressive strengths (72.5 MPa) were recorded. Higher nozzle and platform temperatures, coupled with increased infill rates, enhance layer adhesion, leading to improved tensile and compressive strength. However, with a nozzle temperature of 400°C, platform temperature of 130°C, and 60% infill rate, demonstrating optimal bonding between layers and leads to reduction in warpage. Considering warpage in all four corners and mechanical properties, 400°C nozzle temperature, 0.16 mm layer thickness, 130°C platform temperatures, coupled with 60% infill rates, shows optimal printing conditions. The 10% carbon fiber-reinforced PEEK composites exhibit improved tensile strength 1.68 times compared to pure PEEK. To emphasize the importance of thermal and structural settings, the findings highlight the crucial role of printing parameters in minimizing warpage and enhancing mechanical properties in 3D-printed PEEK parts that is analyzed by multi-objective optimization method. The Scanning Electron Microscopy Analysis were carried out to analyze the fracture morphology and printing layers orientation.

Keywords: Additive Manufacturing (AM); Poly-Ether-Ether-Ketone (PEEK); Fused Deposition Modeling (FDM); Warpage. ANOVA; MOOM

1. Introduction

Over the past decade, 3D printing has become a vital tool in manufacturing due to its efficiency, affordability, and rapid prototyping capabilities, allowing designers to refine models without disrupting main production lines [1]. Among various techniques, Fused Deposition Modeling (FDM) is the most widely used due to its cost-effectiveness and ease of operation. It employs thermoplastic filaments like PLA, ABS, and PEEK, which are melted and extruded layer by layer to form solid structures [2–6]. However, the quality of printed components depends on key parameters such as

 doi:10.20944/preprints202504.1706.v1

printing temperature, layer thickness, and infill percentage, which influence mechanical strength and durability [7–9].

Additive manufacturing, including FDM, enables automated and precise fabrication of complex geometries directly from CAD models. High-performance polymers like PEEK, known for excellent mechanical properties and thermal stability, are increasingly used in advanced applications requiring superior strength and heat resistance [10–13]. Innovations in composite materials, such as resin-based and hybrid CAD/CAM options, have improved dental prostheses' functionality, durability, and cost-efficiency [13,14]. Studies have shown that optimizing conditions, such as a nozzle temperature of 440°C and a controlled printing speed of 20 mm/s, enhances the density and integrity of PEEK components. With the rising demand for high-quality 3D-printed parts, continuous material and process improvements are necessary. PEEK is also replacing metals in some industries due to its exceptional thermal and mechanical properties. It is biocompatible, with a Young's modulus of approximately 3.6 GPa and a tensile strength between 90-100 MPa, making it comparable to compact bone [15,16]. This helps address stiffness mismatches and stress-shielding in medical implants while allowing easy bone growth evaluation due to its radiolucency [17,18].

A major challenge in FDM printing is warping, caused by uneven cooling and shrinkage, leading to dimensional inaccuracies and print failures [19,20]. Studies have investigated factors contributing to warping, including material properties, printing parameters, and environmental conditions [21]. Warping varies across materials; ABS is highly susceptible due to significant shrinkage, whereas PLA exhibits minimal warping due to its lower thermal expansion [22]. Moisture absorption also impacts print quality, affecting extrusion and increasing warping [23]. Researchers have explored composite materials and modified filament compositions to improve dimensional stability [24].

Printing parameters such as bed temperature, nozzle temperature, and print speed significantly affect warping. Higher bed temperatures improve adhesion, reducing thermal stress, while optimized nozzle temperatures enhance layer bonding without excessive extrusion or degradation [25,26]. Print speed also plays a role, as rapid cooling at high speeds increases thermal gradients and residual stress, whereas slower speeds allow more uniform cooling [27]. Environmental factors like ambient temperature and air circulation influence warping, and enclosed print chambers with active heating help maintain temperature stability [28,29]. Post-processing methods like annealing can relieve residual stresses and enhance mechanical properties [30]. Software advancements, such as slicing algorithms and adaptive slicing techniques, further help mitigate warping by optimizing toolpaths and layer adhesion [31,32]. Additionally, raft and brim structures enhance print bed adhesion, reducing warping [33]. Despite these improvements, warping remains a challenge, necessitating ongoing research into novel solutions and materials, including self-healing smart materials and hybrid manufacturing approaches that combine FDM with laser sintering and ultrasonic welding [34,35]. Future directions should focus on real-time monitoring using AI and machine learning to predict and compensate for warping dynamically, ensuring consistent print quality [36].

The impact of printing parameters on warpage in 3D-printed PEEK parts is critical for improving the performance of this high-performance thermoplastic. PEEK's high shrinkage rates during cooling can lead to dimensional inaccuracies and compromised mechanical properties. Understanding the interplay between extrusion temperature, print speed, layer height, and build plate temperature is essential to optimizing print quality. While previous research has explored individual parameters, a gap remains in understanding their combined effects on warpage in industrial applications. Additionally, the absence of standardized methodologies for measuring warpage limits the comparability of findings across studies. This research systematically investigates the combined effects of multiple printing parameters on warpage in 3D-printed PEEK parts, aiming to improve dimensional accuracy through optimized conditions and standardized measurement approaches. This study uniquely examines the combined effects of multiple printing parameters on warpage in PEEK components, addressing the lack of standardized methodologies for measurement and improving reproducibility. By offering industry-relevant recommendations, it enhances the

 doi:10.20944/preprints202504.1706.v1

understanding of high-performance polymer behavior in additive manufacturing, benefiting aerospace, automotive, and medical applications.

2. Materials and Methods

2.1. Materials

For the present study, KetaSpire® PEEK is procured from Solvay, USA. PEEK filament is used to fabricate the model; the properties are that it has a natural color, a diameter of 1.75 mm, and a tolerance of ±0.05 mm. Step-growth polymerization is used to create PEEK polymers.

The ADVANCE HYREL 3D desktop FDM 3D printer was utilized in this investigation. technical specifications are shown in Table 1. Fused Deposition Modeling (FDM) is a widely used 3D printing technology that builds parts by layering melted material. FDM printers use thermoplastic materials, which can be melted and re-solidified. These materials come in filament form, spooled and loaded into the printer. Commonly used filaments include PLA, ABS, PETG, and high-performance plastics such as Polyether ether ketone (PEEK).

Table 1. Technical parameters of Composite 3D printer used in the present study.

Make	Hydra 16 AS
Hot End Type	Bowden Type and Dual Nozzle
Print Process	Fused Filament Fabrication or Fused Deposition Modelling
Resolution	Along the XY platform (15 μm) and along the Z direction (5 μm)
Minimum Layer Thickness	50 μm
Print Speed	250 mm/s
Build Temperature Type	Temperature Monitored Enclosed Chamber
Maximum Chamber Temperature	90°C
Maximum platform Temperature	150°C
Platform Levelling	Kinematic Auto Bed Levelling
Maximum Extrusion Temperature	450°C
Build Platform	Ceramic Glass
Filament Storage	Enclosed Bay with Moisture Control
Air Filtration Unit	HEPA H13 and Activated Carbon Filter
Print Material	PEEK, PLA, ABS, PETG
Bed Size	600 x 400 x 250 mm^3

2.2. Processing of samples

Figure 1 illustrates the methodology adopted in this study. The approach follows a systematic process for 3D printing, tensile, compressive, and warpage measurement. The process begins with the creation of a CAD model, which serves as the digital blueprint for the printed object. Next, key process parameters are defined, including layer height, infill density, bed temperature, and nozzle temperature, all of which significantly influence the quality and structural integrity of the final print. Once these parameters are set, the model undergoes slicing, where it is converted into a machine-readable format for the 3D printer. The printing process is then executed using the optimized settings. Finally, the printed object is evaluated through warpage measurement to analyze any deformations caused by thermal stresses and material shrinkage. This structured methodology ensures an efficient and optimized workflow, leading to high-quality 3D-printed components with minimal warpage.

A 3D cuboid model in STL format was created with dimensions of 100 mm in length, 30 mm in width, and 5 mm in height is used for warpage study. The STL (Stereolithography) file format is a widely used format in 3D systems CAD (Computer-Aided Design) software. It is commonly utilized

 doi:10.20944/preprints202504.1706.v1

in rapid prototyping and Computer-Aided Manufacturing (CAM) and is supported by many other software programs. Next, the digital model is processed using slicing software, such as Slicer, which converts it into thin-layer printing instructions for an open-source FDM 3D printer. This process generates a G - Code (G-Programming Language) file, which contains all the commands and instructions required by the 3D printer. The G - Code file directs the extrusion head of the FDM 3D printer, specifying its precise motion control paths. The FDM 3D printer builds the physical object by depositing material in successive thin horizontal cross-sections, following the G-Code instructions. The raw PEEK material is extruded through a circular nozzle, which moves horizontally in a piecewise linear path for each layer. After extruding the material along each line segment, the next layer is deposited once the previous layer has been completed. Either the printing platform or the circular nozzle moves vertically to continue the process. This layer-by-layer approach allows for the fabrication of complex 3D geometries, making it an efficient method for producing intricate 3D-printed components. FDM 3D fabrication is an additive manufacturing process where material is systematically deposited layer by layer to create a 3D object. The process starts with a digital CAD model, which is converted into an STL file and then processed using slicing software to generate layer-by-layer printing instructions. A thermoplastic filament like PEEK is heated in the extruder to its melting point (400°C – 420°C) and deposited onto a carbon fiber bed, which ensures even heat distribution. As each layer is deposited and solidified, it bonds with the previous layer, gradually forming the final 3D object.

Table 1 presents the technical parameters of composite 3D printer. In this study, nine FDM 3D-printed specimens were fabricated and analyzed. Table 2 refers constant parameters used in this work. Each specimen was printed with a flat orientation and a raster angle of +45°/-45° to the X-axis. This alternating raster pattern was selected over a unidirectional orientation, as it is the standard printing strategy for most FDM 3D-printed objects. Consequently, the manufacturing process of the FDM 3D-printed parts is directly linked to the results of this study.

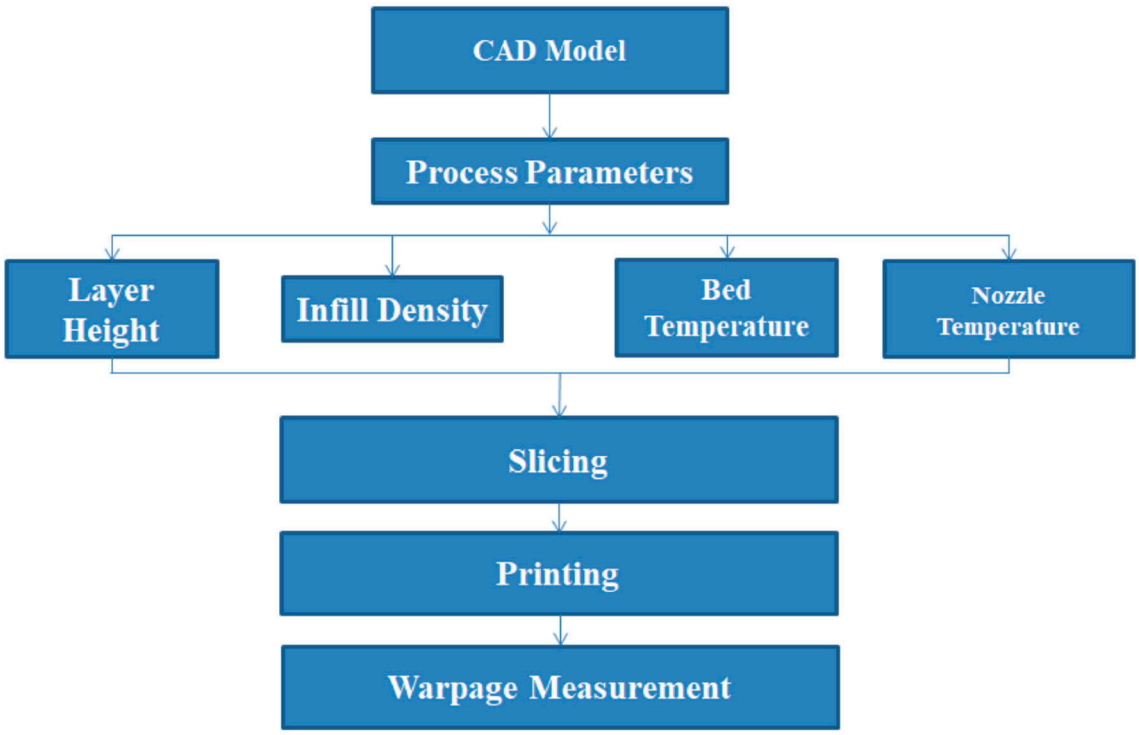

Figure 1. Methodology to evaluate tensile, compression and warpage properties.

 doi:10.20944/preprints202504.1706.v1

Table 2. Constant parameters.

Technology	FDM (Fused Deposition Modeling)
Filament Diameter	1.75 mm
Nozzle Diameter	0.4 mm
Material Type	PEEK
File Compatibility	STL and G-code
Print Speed	20 mm/sec
Raster Angle	±45°
Chamber Temperature	60 °C
Printing Size (l × b × h)	100×30×5 mm
Internal (Infill) Structure	Rectilinear

In FDM 3D printing, nozzle temperature refers to the controlled heat applied to the nozzle to melt the thermoplastic filament, enabling precise layer-by-layer deposition. Layer height is the thickness of each deposited layer, which affects the print resolution, surface finish, and overall print time. Bed temperature is the heat maintained on the build platform to ensure proper adhesion of the first layer, reduce warping, and improve print quality. Infill percentage determines the density of the internal structure, with higher percentages resulting in stronger but heavier prints. Printing speed, measured in mm/s, refers to how quickly the 3D printer extrudes material, directly impacting print quality and efficiency. Lastly, chamber temperature is the controlled environment within the build chamber, crucial in FDM and SLS 3D printing, as it influences material behavior and print quality. In the experimental trial runs, different values of nozzle temperature, layer thickness, platform temperature, and infill rate were considered shown in Table 3. These parameters were found to have the most significant impact on the construction of parts in FDM 3D printing technology. The FDM 3D printing process parameters used in this study are presented in Table 4, which includes the independent variables (nozzle temperature, layer thickness, platform temperature, and infill rate).

Table 3. Control factors and their levels.

Levels Number	Nozzle Temperature (°C)	Layer Height (mm)	Platform Temperature (°C)	Infill Ratio (%)
1	400	0.16	130	60
2	410	0.18	140	80
3	420	0.20	150	100

Table 4. Process parameters selection for desktop FDM 3D printer unit.

Run/ Sample Number	Nozzle Temperature (°C)	Layer Thickness (mm)	Platform Temperature (°C)	Infill Rate (%)
1	400	0.16	130	60
2	400	0.18	140	80
3	400	0.2	150	100
4	410	0.16	140	100
5	410	0.18	150	60
6	410	0.2	130	80
7	420	0.16	150	80
8	420	0.18	130	100
9	420	0.2	140	60

Initially, the samples were prepared to assess the influence of various printing parameters (as listed in Tables 3 and 4) on tensile and compression properties. A total of five identical samples were fabricated and tested under the relevant standards in alignment with the printing direction. Tensile

 doi:10.20944/preprints202504.1706.v1

tests were conducted on the 3D-printed PEEK parts at room temperature, following ISO 527-2 standards shown in Figure 2a. The tests were performed using a Zwick Roell series Z 020 Universal Testing Machine (UTM) equipped with a 20 kN load cell. Tensile strength and elastic modulus were measured at a strain deformation rate of 5 mm/min. For compression tests, the ASTM D695 standard was applied shown in Figure 2b. The compression test was conducted using the Zwick Roell series UTM machine, with a constant displacement rate of 1.50 mm/min. The warpage measurement is shown in Figure 3.

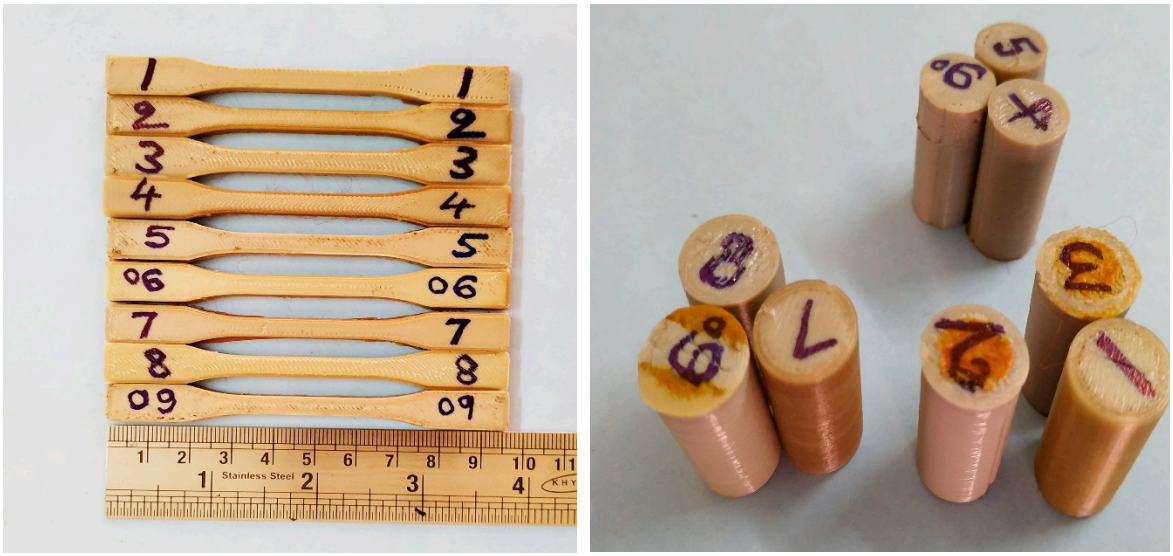

Figure 2. 3D printed PEEK samples a) Tensile specimens b) Compression specimens.

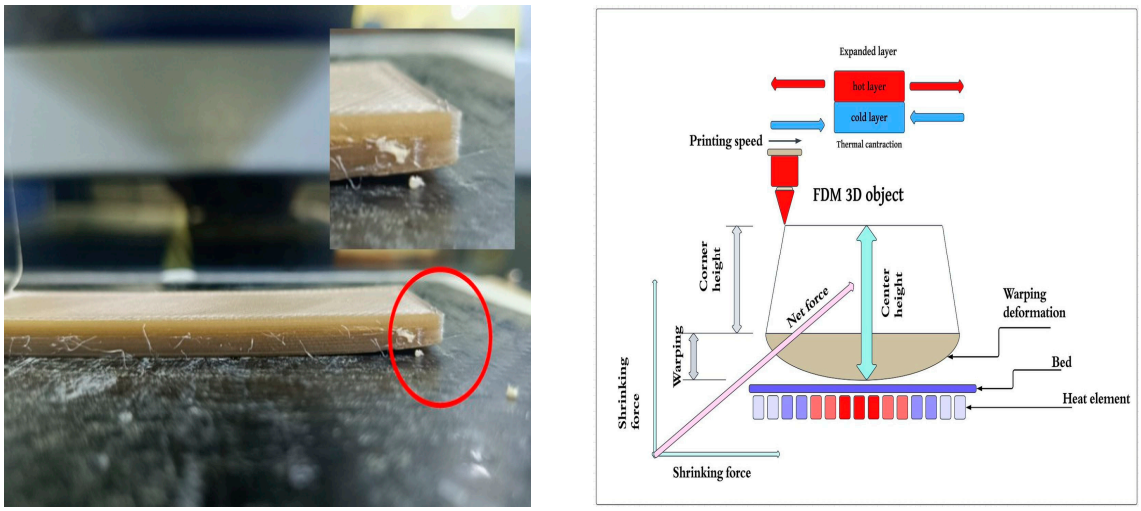

Figure 3. Warpage deformation and its method of measurement at each corner.

3. Results and Discussion

The experiment utilized ImageJ software to measure warping deformation in FDM 3D-printed parts. Warpage occurs due to thermal contraction, impacting print accuracy and mechanical performance. ImageJ, an open-source tool, enables precise image processing, analysis, and measurement of warping effects. Key features include area selection, distance and angle measurements, and 3D visualization capabilities. Proper calibration ensures accurate scaling, making ImageJ a valuable resource for scientific imaging and additive manufacturing research.

 doi:10.20944/preprints202504.1706.v1

3.1. Tensile Properties

The results of the tensile stress at break and strain at break for the nine different samples are presented in the Table 5, showing both the averages and variability across individual measurements. The analysis of these parameters is critical for understanding the material's mechanical properties, particularly its ability to withstand stress before failure and its ductility (strain at break). The variability in both tensile stress and strain indicates the consistency and reliability of the material under different testing conditions. The tensile stress at break measures the maximum stress a material can withstand before breaking. The average tensile stress at break for the samples varied from 45.36 MPa (Sample 1) to 71.4 MPa (Sample 8). Sample 1 exhibited the lowest average tensile stress, while Sample 8 showed the highest. Notably, the tensile stress at break did not vary excessively between the samples, with the standard deviations ranging from 1.202 MPa (Sample 5) to 1.701 MPa (Sample 1), indicating relatively stable performance across all samples. The minimum and maximum values for tensile stress varied across the samples, with Sample 1 showing the narrowest range between the minimum (43 MPa) and maximum (47.2 MPa), suggesting consistent performance. Meanwhile, Sample 9 had a wider range, from 49 MPa to 52 MPa, although the standard deviation of 1.294 MPa indicated some level of consistency in performance across the sample. The strain at break refers to the material's ability to undergo deformation before breaking, providing insights into its ductility. Sample 9 had the highest average strain at break (27.5%), suggesting superior ductility compared to the other samples. In contrast, Samples 2 and 3 exhibited the lowest average strain at break, at 8.26% and 7.4%, respectively, highlighting their relatively brittle nature. The variability in strain at break was also significant across the samples, with Sample 9 having the highest standard deviation of 5.590%, indicating considerable variability in strain behavior. Conversely, Sample 2 had the lowest standard deviation of 1.545%, suggesting a more uniform strain behavior under tensile stress. The maximum tensile strength observed was 71.4 MPa when the nozzle temperature was set to 420°C, with a layer height of 0.18 mm, a bed temperature of 130°C, and an infill density of 100%. Under these conditions, the material demonstrates a high level of mechanical integrity. When 10% carbon fiber-reinforced PEEK (Polyetheretherketone) was printed under identical conditions, the mechanical properties were significantly enhanced. This composite material exhibited a maximum tensile strength of 120.1 MPa, representing a notable increase in strength over the pure PEEK. Additionally, the strain at break—an indicator of the material's ductility—was recorded at 8.85%, implying that the carbon fiber reinforcement improves both strength and flexibility compared to the unreinforced PEEK. This enhanced performance is a direct result of the carbon fibers, which reinforce the polymer matrix, leading to improved load-bearing capacity and better resistance to mechanical failure under stress.

Table 5. Tensile stress and strain.

Run / sample No.	Tensile Stress at Break (MPa)				Strain at Break (%)			
	Average	Minimum	Maximum	Standard deviation	Average	Minimum	Maximum	Standard deviation
1	45.36	47.2	43	1.701	29.4	34	25.5	3.343
2	63.2	64.5	61.5	1.358	8.26	10	6	1.545
3	68.2	70	66	1.605	7.4	10	5	1.935
4	66.04	67.2	64	1.316	11.7	15	9	2.387
5	54.5	56	53	1.202	8.54	11	6	2.170
6	59.46	61	58	1.248	7.1	9	4	1.981
7	52.24	54	50.5	1.383	8.5	11	6	1.904
8	71.4	73	70	1.294	8.24	10	5.5	1.799
9	50.4	52	49	1.294	27.5	35	20	5.590

From the data, it can be observed that while tensile stress at break remained relatively consistent across the samples, strain at break exhibited a greater range of variability. This disparity can be

 doi:10.20944/preprints202504.1706.v1

attributed to the different material compositions and testing conditions, which might have influenced the samples' ductility to a greater extent than their tensile strength. Sample 9 stands out as a particularly interesting case, with both the highest tensile stress at break and the largest variation in strain at break. This suggests that while the material could withstand significant tensile stress before breaking, it demonstrated a wide range of ductility across individual tests. This variability may be a result of factors such as microscopic material flaws, inconsistencies in manufacturing, or differences in testing conditions. On the other hand, Sample 2, despite having a relatively high tensile stress at break (63.2 MPa), displayed a low strain at break (8.26%) and low variability (1.545%), suggesting it is a more brittle material compared to other samples. This could indicate a more rigid structure with less ability to deform plastically before failure.

4.2. Compression Properties

The average compressive stress at break across samples varies from 72.5 MPa to 167 MPa shown in Table 6. While PEEK is a high-performance thermoplastic known for its excellent mechanical properties (including compressive strength). The strain at break shows the amount of deformation each sample can endure before failure. The strain at break ranges from 15.5% to 90%. This variability suggests differences in the ductility of the samples. For PEEK, which typically has relatively low ductility compared to metals, a high strain at break (above 70%) would be atypical. Although PEEK is tough, 3D printed PEEK may show reduced ductility due to layer bonding issues, leading to brittleness. Brittle materials fail suddenly under compressive loading without significant plastic deformation. This is evident in the samples with lower strain at break (e.g., Sample 1, 72.5 MPa, strain at break 25.8%). Higher strain at break could indicate a more ductile sample, which can better absorb energy before failure, but PEEK's behavior in the 3D printed state may lead to inadequate energy absorption capacity under compression if the layers are weakly bonded. The standard deviations in both compressive stress and strain at break suggest significant variability between samples. Some samples (e.g., Sample 4 and Sample 8) have a strain at break close to 80-90%. While these numbers are high, it's important to note that they may reflect the material's capability to deform in compression before failure. However, this can also indicate that the material is undergoing significant deformation before breaking, which is not ideal for compressive strength under loads where minimal deformation is desirable. Even though some samples show high strain at break, they might still fail under prolonged compressive loads due to issues like creep or buckling. 3D printed PEEK, especially under elevated temperatures or constant compressive forces, may start to deform plastically over time, leading to failure even if initial compressive strength seems adequate.

Table 6. Compressive stress and strain.

Run/ sample No.	Compression Stress at Break (MPa)				Strain at Break (%)			
	Average	Minimum	Maximum	Standard deviation	Average	Minimum	Maximum	Standard deviation
1	104.2	108	100	3.094	21.7	30	15.5	5.805
2	116.2	119	113	2.564	34	41.5	27.5	6.548
3	120.6	123.5	118	2.162	32.1	39	22	7.215
4	167	173	160	4.950	78	90	65	10.368
5	113.4	116	111	1.981	44.4	55	35	8.112
6	116.1	118	114	1.517	43	55	30	9.906
7	115.8	118	113	2.080	28.2	38	18	8.438
8	164.4	168	160	3.453	73	85	60	10.368
9	72.5	75	70	2.062	25.8	35	18	6.723

The variation in compressive and tensile stress observed in the 3D-printed samples can be attributed to differences in printing conditions such as nozzle temperature, layer thickness, platform temperature, and infill rate. Nozzle temperature plays a critical role in material flow and layer

 doi:10.20944/preprints202504.1706.v1

adhesion, with higher temperatures (e.g., 420°C) generally improving interlayer bonding, which enhances strength but may also introduce residual stresses leading to variations in performance. Layer thickness affects the mechanical properties by influencing the bonding between adjacent layers; thinner layers (e.g., 0.16 mm) typically result in better adhesion but may introduce stress concentrations, while thicker layers (e.g., 0.2 mm) can lead to weaker bonding between layers, reducing mechanical strength. Platform temperature is another significant factor as higher temperatures (e.g., 150°C) help reduce thermal gradients, minimizing warpage and improving overall part integrity, while lower temperatures (e.g., 130°C) may cause uneven cooling and induce internal stresses that weaken the part. Additionally, the infill rate directly impacts the density and mechanical performance of the printed parts, with higher infill percentages (e.g., 100%) providing more material support and increasing compressive and tensile strength, while lower infill rates (e.g., 60%) introduce internal voids, reducing the overall mechanical resistance. The interplay of these parameters leads to the observed variations in stress, as seen in samples with higher temperatures and optimized conditions (e.g., Sample 4 and 8) exhibiting greater strength, while those with suboptimal parameters (e.g., Sample 9) show lower stress values due to insufficient bonding and structural inconsistencies. The maximum compression strength and strain of PEEK were found to be 164.4 MPa and 73%, respectively, at a nozzle temperature of 420°C. The test was conducted with a layer height of 0.18 mm, a bed temperature of 130°C, and an infill density of 100%. For the 10% carbon fiber-reinforced PEEK, printed under the same conditions, the mechanical performance was significantly enhanced. The maximum tensile strength increased to 171.32 MPa, while the strain at break decreased to 59.42%.

The variation in tensile and compressive loading properties across different groups is influenced by printing parameters such as nozzle temperature, layer thickness, platform temperature, and infill rate shown in Table 7. Higher nozzle temperatures and optimal platform temperatures improve interlayer adhesion, enhancing both tensile and compressive strength, as seen in Group 8. Groups with lower infill rates and suboptimal thermal conditions exhibit reduced mechanical performance due to weaker bonding and increased voids, as observed in Group 9. Variations in strain indicate differing material deformation behavior, with higher strain in compressive loading reflecting improved ductility under specific conditions. Unreinforced PEEK has a tensile strength of 71.4 MPa and good mechanical integrity. Carbon fiber-reinforced PEEK exhibits a tensile strength of 120.1 MPa and a reduced strain at break of 8.85%. The carbon fibers enhance strength but reduce flexibility compared to pure PEEK. The PEEK shows a compression strength of 164.4 MPa and a high strain at break of 73%. When reinforced with 10% carbon fiber, the tensile strength increases to 171.32 MPa, but the strain at break drops to 59.42%.

Table 7. Variance and standard deviation in tensile and compressive loading for various samples.

		Tensile loading						Compressive loading					
		Stress (MPa)			Strain (%)			Stress (MPa)			Strain (%)		
Groups	*Count*	*Sum*	*Average*	*Variance*	*Sum*	*Average*	*Variance*	*Sum*	*Average*	*Variance*	*Sum*	*Average*	*Variance*
1	5	226.8	45.36	2.893	147	29.4	11.175	521	104.2	9.575	108.5	21.7	33.7
2	5	316	63.2	1.845	41.3	8.26	2.388	581	116.2	6.575	170	34	42.875
3	5	341	68.2	2.575	37	7.4	3.745	603	120.6	4.675	160.5	32.1	52.05
4	5	330.2	66.04	1.733	58.5	11.7	5.7	835	167	24.5	390	78	107.5
5	5	272.5	54.5	1.445	42.7	8.54	4.708	567	113.4	3.925	222	44.4	65.8
6	5	297.3	59.46	1.558	35.5	7.1	3.925	580.5	116.1	2.3	215	43	98.125
7	5	261.2	52.24	1.913	42.5	8.5	3.625	579	115.8	4.325	141	28.2	71.2
8	5	357	71.4	1.675	41.2	8.24	3.238	822	164.4	11.925	365	73	107.5
9	5	252	50.4	1.675	137.5	27.5	31.25	362.5	72.5	4.25	129	25.8	45.2

3.3. Warpage

Figure 4a shows the sample with corner mentioned for measurement and Figure 4b shows the warpage measurement of sample using ImageJ software. The measurement is done with linear and angular dimension, to assess the impact of various printing parameters on the warpage behavior of

 doi:10.20944/preprints202504.1706.v1

PEEK samples. The warpage of the samples was analyzed by measuring the dimensions of the test bar at each corner (A, B, C, and D) using ImageJ software. Each dimension at the corners was measured at least three times, and the average (mean) and standard deviation were calculated. The deviation for each dimension (corner) of the test bar was then computed.

Table 8 and Figure 5 show the warpage measurements for the samples at different corners in mm. It is evident that the maximum warpage is observed in sample 3 (Nozzle temperature: 400°C, Layer thickness: 0.2 mm, Platform temperature: 150°C, and Infill rate: 100%) with a magnitude of 6.09 mm at corner A. The maximum warpage at corner B (6.43 mm) is also observed in sample 3. In sample 5 (Nozzle temperature: 410°C, Layer thickness: 0.18 mm, Platform temperature: 150°C, and Infill rate: 60%), the maximum warpage of 6.63 mm is observed at corner C. The maximum warpage at corner D (7.89 mm) is also found in sample 5. Figure 4a shows sample 9 with corners A, B, C, and D used to measure warpage in mm using ImageJ software. It also shows the relationship between the average value and different samples. Sample 5, with printing parameters of a nozzle temperature of 410°C, layer thickness of 0.18 mm, platform temperature of 150°C, and an infill rate of 60%, shows the highest warpage, while Sample 1, with nozzle temperature 400°C, layer Pthickness of 0.16 mm, platform temperature 130°C, and infill rate 60%, exhibits the lowest Pwarpage.

Table 9 and Figure 6 show the warpage measurements for the samples at different corners in degrees. The results indicate that Sample 5 shows a significant mean warpage of 18.7°, while Sample 1 shows a much lower mean warpage of 3.35°. This difference can be attributed to the higher nozzle temperature used in Sample 5 (410°C) compared to Sample 1 (400°C). Higher nozzle temperatures increase thermal gradients between the printed layers, resulting in more pronounced warpages due to uneven cooling and contraction between layers. It is evident that the maximum warpage occurs in Sample 9 (Nozzle temperature: 420°C, Layer thickness: 0.2 mm, Platform temperature: 140°C, and Infill rate: 60%) with an angle of 22° at corner A. On the other hand, the minimum warpage is observed in Sample 1 (Nozzle temperature: 400°C, Layer thickness: 0.16 mm, Platform temperature: 130°C, and Infill rate: 60%) with an angle of 3.3° at corner A. At corner B, the maximum warpage (15.5°) is observed in Sample 4 (Nozzle temperature: 410°C, Layer thickness: 0.16 mm, Platform temperature: 140°C, and Infill rate: 100%), while the minimum warpage (5.7°) is seen in Sample 7 (Nozzle temperature: 420°C, Layer thickness: 0.16 mm, Platform temperature: 150°C, and Infill rate: 80%). At corner C, the maximum warpage (21.6°) is observed in Sample 5 (Nozzle temperature: 410°C, Layer thickness: 0.18 mm, Platform temperature: 150°C, and Infill rate: 60%), while the minimum warpage (1.6°) is observed in Sample 1. Similarly, at corner D, the maximum warpage (23.2°) is recorded in Sample 5, whereas the minimum warpage (2.1°) is observed in Sample 2.

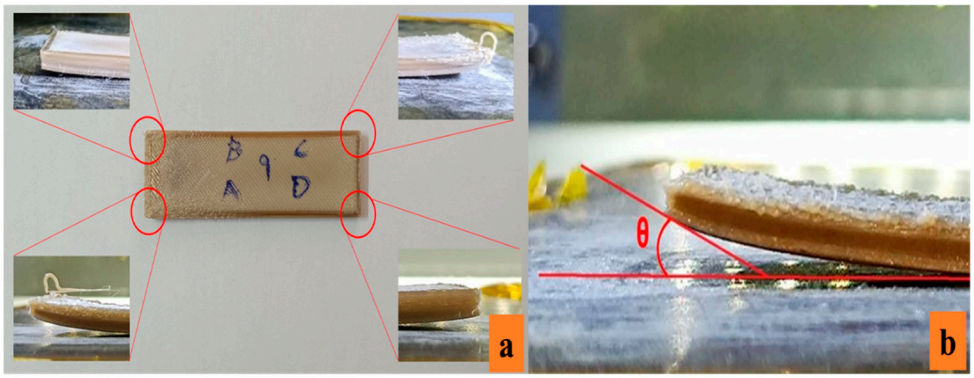

Figure 4. (a) Warpage of sample 9 showing different corners (b) Warpage measurement in degrees using ImageJ software.

 doi:10.20944/preprints202504.1706.v1

Table 8. Warpage at each corner of the samples in mm.

Sample No.	Corner A	Corner B	Corner C	Corner D	Average
1	1.46	1.30	0.83	0.61	**1.05**
2	1.80	2.73	1.78	0.97	**1.82**
3	6.09	6.43	2.06	2.07	**4.16**
4	4.53	4.47	3.70	2.87	**3.89**
5	6.02	2.95	6.63	7.89	**5.87**
6	3.43	3.11	1.72	1.10	**2.34**
7	1.44	1.38	1.65	1.47	**1.49**
8	4.97	4.42	3.85	4.54	**4.45**
9	4.48	3.82	2.08	2.15	**3.13**
Average	**3.80**	**3.40**	**2.70**	**2.63**	

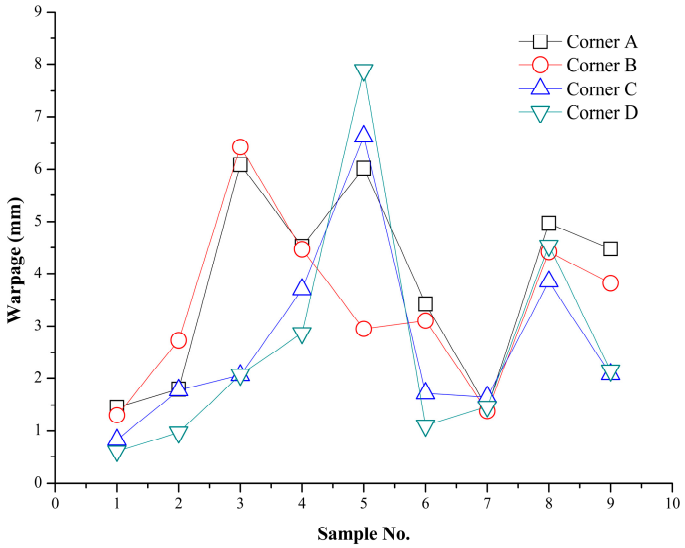

Figure 5. Warpage at each corner of the samples in mm.

Table 9. Warpage at each corner of the samples in degrees.

Sample No.	Corner A	Corner B	Corner C	Corner D	Average
1	3.3	6.3	1.6	2.2	**3.35**
2	4.9	7.5	4.4	2.1	**4.72**
3	20.7	13.4	8.8	5.5	**12.10**
4	19.6	15.5	11.2	11.5	**14.45**
5	17.2	12.8	21.6	23.2	**18.70**
6	10.8	10.6	7.6	5.9	**8.72**
7	6.0	5.7	6.4	5.5	**5.90**
8	21.9	12.0	13.5	21.1	**17.12**
9	22.0	11.7	9.6	11.4	**13.67**
Average	**14.04**	**10.61**	**9.41**	**9.82**	

 doi:10.20944/preprints202504.1706.v1

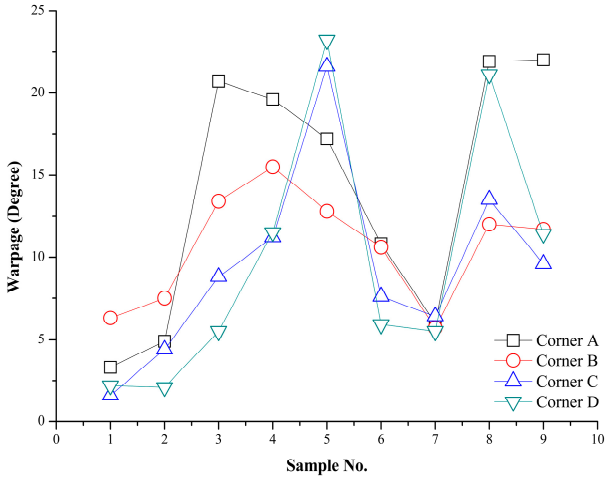

Figure 6. Warpage at each corner of the samples in degrees.

Figure 7 shows the linear warpage of Sample 1 and Sample 2 along the length of the samples (100 mm). In Sample 1, the warpage at corner A is 1.46 mm, and at corner D it is 0.61 mm. In Sample 2, the warpage at corner A is slightly higher at 1.80 mm, and at corner D it is 0.97 mm. The increased warpage in Sample 2 suggests that the change in printing parameters (such as nozzle temperature) affects the overall deformation of the sample, with Sample 2 exhibiting slightly more warpage across both corners compared to Sample 1.

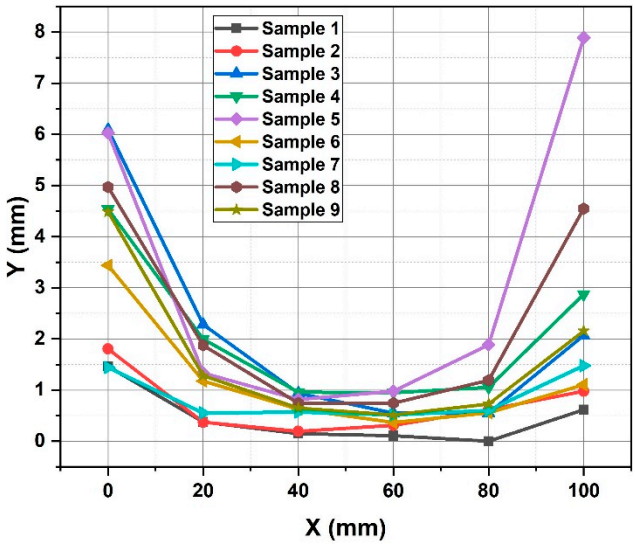

Figure 7. Warpage analysis of samples with respect to X and Y direction.

In Sample 3, the warpage at corner A is 6.09 mm, and at corner D it is 2.07 mm. Sample 4, with a slightly different printing parameter set, shows warpage at corner A of 4.53 mm and at corner D of 2.87 mm. The greater warpage at corner A in Sample 3 (6.09 mm vs. 4.53 mm in Sample 4) and the slightly higher warpage at corner D in Sample 4 (2.87 mm vs. 2.07 mm in Sample 3) suggest that variations in nozzle temperature, layer thickness, and infill rate significantly influence the degree of warpage, particularly in the earlier and later printed layers of the sample.

In Sample 5, the warpage at corner A is 6.02 mm, while at corner D it is much larger, measuring 7.89 mm. In Sample 6, the warpage at corner A is 3.43 mm, and at corner D it is significantly lower at 1.10 mm. Sample 5, with a higher nozzle temperature and a different layer thickness, exhibits considerably more warpage, especially at corner D, indicating that higher temperatures and thinner layers contribute to increased deformation due to more significant thermal gradients during the

 doi:10.20944/preprints202504.1706.v1

printing process. On the other hand, Sample 6 shows lower warpage, particularly at corner D, suggesting that certain printing settings may reduce the warpage effect.

In Sample 7, the warpage at corner A is 1.44 mm, and at corner D it is 1.47 mm. In Sample 8, corner A shows warpage of 4.97 mm, while corner D shows 4.54 mm. The warpage in Sample 7 is relatively low, especially at corner A, suggesting minimal thermal deformation. In contrast, Sample 8 demonstrates higher warpage at both corners, indicating that the higher nozzle temperature (420°C) in Sample 8 leads to a greater temperature differential and, consequently, more warping.

In sample 9, at corner A, the warpage is 4.48 mm, while at corner D it is 2.15 mm. This sample, which has the highest nozzle temperature of 420°C, exhibits moderate warpage compared to Sample 5, but still shows notable deformation, particularly at corner A, where higher temperatures result in a more pronounced warpage effect. 10% carbon fiber-reinforced PEEK exhibits warping at four corners: Corner A (4.32°), Corner B (5.21°), Corner C (1.85°), and Corner D (1.96°). The warpage at each corner measures 1.24 mm, 1.12 mm, 1.32 mm, and 1.14 mm, respectively. Despite this warping, the dimensional stability of carbon fiber-reinforced PEEK is improved compared to neat PEEK, indicating better resistance to deformation during the solidification process after each printing layer. The reduction in warpage at each corner highlights the reinforcement's effectiveness in enhancing stability. Overall, the material demonstrates significant improvement in maintaining shape during processing.

3.3. Multi-objective optimization technique

The Criteria Importance Through Inter-criteria Correction (CIC) method is used to calculate the weights for processing parameters based on their impact on multiple objectives, such as maximizing tensile and compressive stress and minimizing warpage. The Preference Selection Index (PSI) ranks the processing conditions by evaluating their effectiveness in achieving these objectives. Table 10 shows the calculated weights as per CIC methods. Table 11 shows different combinations of nozzle temperature, layer thickness, platform temperature, and infill rate with their corresponding ranks. Rank 1 represents the best combination of processing parameters, while Rank 9 indicates the least optimal combination. The results show that Sample 1 (400°C nozzle, 130°C platform, 0.16 mm layer thickness, 60% infill) achieved the best performance, likely due to minimal thermal stress and balanced adhesion. Sample 7 (420°C, 150°C, 0.16 mm, 80% infill) also performed well, ranking second, suggesting that higher temperatures with moderate infill improve mechanical strength. Conversely, Sample 9 (420°C, 140°C, 0.2 mm, 60% infill) ranked lowest, indicating that excessive temperature and low infill reduce structural stability. These findings highlight the importance of optimizing multiple parameters to achieve high-quality PEEK prints.

Table 10. Weight calculation for each objective parameter.

Name		Cj	Weights
Tensile	Stress	2.573264	**0.069236**
	Strain	3.498358	**0.094127**
Compression	Stress	2.674397	**0.071957**
	Strain	5.803776	**0.156157**
Warpage at each corner in mm	A	2.630422	**0.070774**
	B	2.269163	**0.061054**
	C	2.325958	**0.062582**
	D	2.474688	**0.066584**
Warpage at each corner in degrees	A	2.906478	**0.078202**
	B	2.354517	**0.063351**
	C	4.824957	**0.129821**
	D	2.830365	**0.076154**
Sum of weights			**1**

 doi:10.20944/preprints202504.1706.v1

Table 11. Multi-objective optimization methods and their ranking.

Run / sample number	Nozzle Temperature (°C)	Layer Thickness (mm)	Platform Temperature (°C)	Infill Rate (%)	Ranks
1	400	0.16	130	60	**1**
2	400	0.18	140	80	**3**
3	400	0.2	150	100	**5**
4	410	0.16	140	100	**7**
5	410	0.18	150	60	**8**
6	410	0.2	130	80	**4**
7	420	0.16	150	80	**2**
8	420	0.18	130	100	**6**
9	420	0.2	140	60	**9**

3.4. Scanning Electron Microscopy

To analyze the morphology of 3D printed PEEK components, fracture surfaces of tensile specimens are examined. In compression testing, different failure modes were observed among the specimens. Some samples exhibited layer delamination, where the individual printed layers separated due to insufficient adhesion or excessive internal stresses. This failure mode is commonly seen in anisotropic materials like 3D-printed PEEK, where weak interlayer bonding can lead to structural failure under compressive loads. Other specimens, however, did not rupture completely but experienced progressive deformation, where the layers deteriorated and bulged outward instead of fracturing. The red arrows in Figure 9a,b highlight these bulging effects, which indicate plastic deformation under high compressive stress. This type of failure is influenced by printing parameters such as nozzle temperature, cooling rate, and layer adhesion. Similar findings were reported by Ren [37], confirming that compression failure in PEEK parts is highly dependent on process parameters and layer bonding quality. For tensile testing, specimens No. 1 and No. 8 were selected to analyze the impact of process parameters on mechanical performance. Figure 9 shows the fractured PEEK specimens post-tensile testing, highlighting the differences in failure modes. Lower strength specimens (Figure 9a,b,c) exhibit defects such as voids, interlayer separation, and weak fusion lines. These defects arise due to insufficient nozzle temperature, which leads to incomplete melting and poor filament adhesion. Additionally, micro-voids and uneven material distribution can occur, further weakening the printed structure. Higher strength specimens (Figure 9d,e) show superior bonding and fewer defects. The use of higher nozzle temperatures improves material fluidity, allowing better fusion between layers and stronger filament-to-filament bonding. This leads to enhanced tensile properties, as the interlayer adhesion can withstand higher loads before failure.

 doi:10.20944/preprints202504.1706.v1

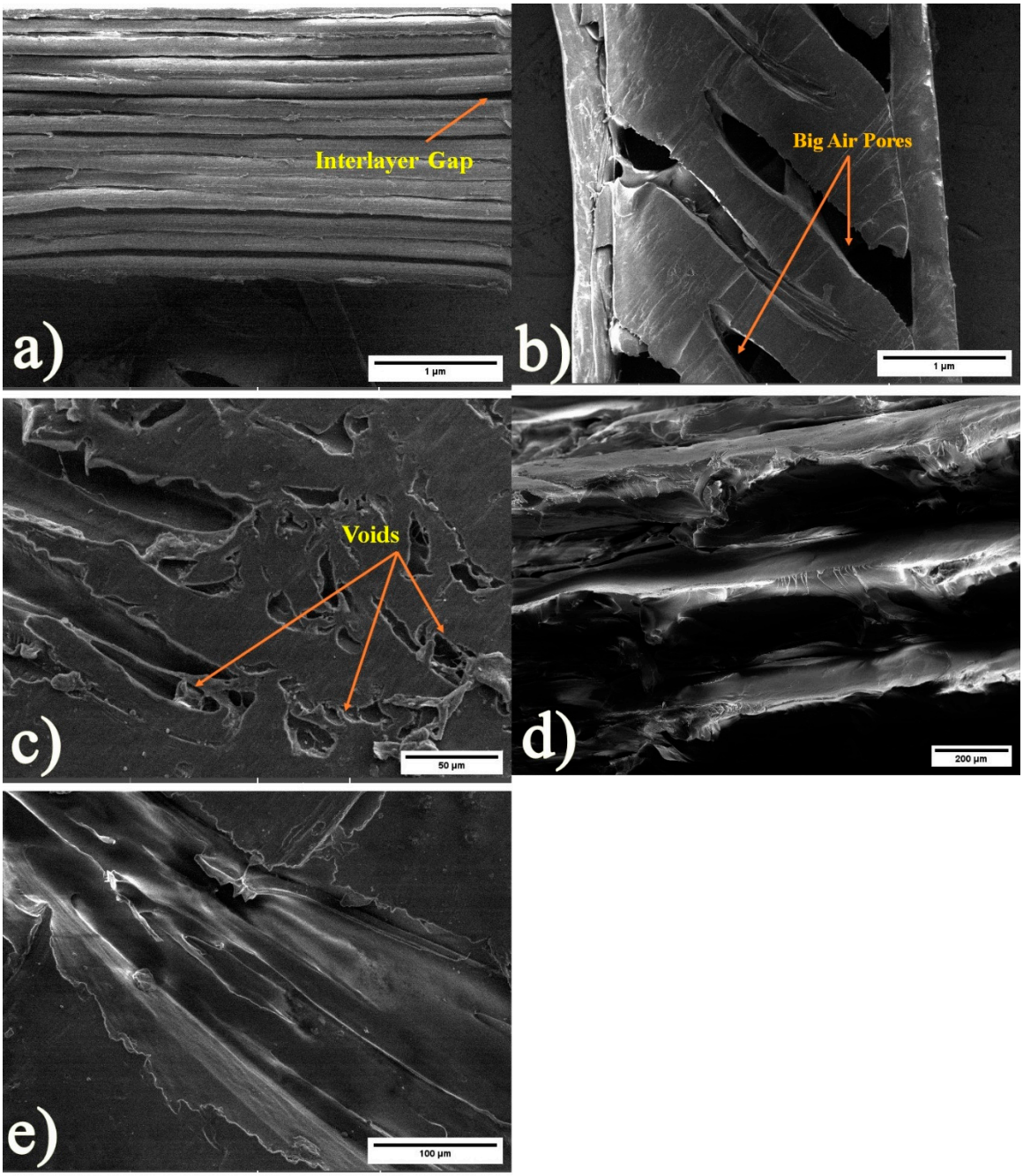

Figure 9. SEM micrographs of the tensile fracture surface of 3D printed PEEK at (a, b, c) 400°C, and (d, e) 420°C.

4. Conclusions

The mechanical performance and structural integrity of 3D-printed PEEK components are significantly influenced by process parameters such as nozzle temperature, platform temperature, layer thickness, and infill rate. This study systematically evaluated these parameters to determine their effects on tensile and compression strength, strain behavior, warpage, and fracture characteristics.

- Optimal tensile performance was achieved with a nozzle temperature of 420°C, a platform temperature of 130°C, and an 80–100% infill rate, resulting in improved interlayer bonding and higher tensile strength (71.4 MPa). Compression strength was maximized at 167 MPa with higher nozzle temperatures, which facilitated better filament fusion. Warpage analysis

 doi:10.20944/preprints202504.1706.v1

revealed that dimensional stability was enhanced by optimizing temperature settings, with minimal distortion occurring at lower warpage values. Multi-objective optimization ranked Sample No. 1 as the best-performing specimen due to its balanced mechanical properties, minimal deformation, and enhanced fracture resistance.

- The highest warpage due to high temperature and low infill, sample 5 exhibited the highest linear (7.89 mm at corner D) and angular warpage (23.2° at corner D), indicating strong sensitivity to high nozzle temperature (410°C) and low infill rate (60%). Sample 1 showed the lowest warpage, with values as low as 0.61 mm (corner D) and 3.3° (corner A), demonstrating optimal dimensional stability under reduced temperature and thicker layers. Carbon fiber-reinforced PEEK reduced warpage significantly, with maximum values of 1.32 mm and 5.21°, confirming enhanced thermal stability over neat PEEK.
- Fracture image analysis confirmed that higher-strength specimens exhibited fewer voids, better fusion, and stronger bonding, while lower-strength specimens displayed interlayer separation and weak adhesion. Additionally, the inclusion of 10% carbon fiber reinforcement improved tensile properties and dimensional stability, while reducing ductility, with no significant effect on compression strength.
- These findings provide key insights into optimizing 3D printing parameters for PEEK and its composites, ensuring improved mechanical performance and structural integrity for advanced engineering applications.

Key Takeaways and Future Recommendations

- Higher nozzle temperatures improve interlayer bonding and reduce defects.
- Optimized cooling strategies can further enhance structural integrity.
- Post-processing treatments such as annealing may enhance mechanical properties.
- Future studies should explore hybrid infill patterns to balance strength and weight.

Funding: The authors wish to sincerely acknowledge the financial support from the Science and Engineering Research Board - Department of Science and Technology (EEQ/2021/000763), New Delhi, Government of India and IDEA2PoC Grant Scheme (Elevate-Unnati 2021) of Karnataka Startup Policy, KITS, Dept. of Electronics, IT, Bt and S&T Govt. of Karnataka.

References

1. Sapata, A.; Šinka, M.; Šahmenko, G.; Korat Bensa, L.; Hanžič, L.; Šter, K.; Ručevskis, S.; Bajāre, D.; Bos, F.P. Establishing Benchmark Properties for 3D-Printed Concrete: A Study of Printability, Strength, and Durability. J. Compos. Sci. 2025, 9, 74. https://doi.org/10.3390/jcs9020074
2. Indreș, A.I.; Constantinescu, D.M.; Mocian, O.A.; Sorohan, Ș. Particularities on the Low-Velocity Impact Behavior of 3D-Printed Sandwich Panels with Re-Entrant and Honeycomb Core Topologies. J. Compos. Sci. 2024, 8, 426. https://doi.org/10.3390/jcs8100426
3. Anwajler, B.; Szulc, P. The Impact of 3D Printing Technology on the Improvement of External Wall Thermal Efficiency—An Experimental Study. J. Compos. Sci. 2024, 8, 389. https://doi.org/10.3390/jcs8100389
4. Ogaili, A.A.F.; Basem, A.; Kadhim, M.S.; Al-Sharify, Z.T.; Jaber, A.A.; Njim, E.K.; Al-Haddad, L.A.; Hamzah, M.N.; Al-Ameen, E.S. The Effect of Chopped Carbon Fibers on the Mechanical Properties and Fracture Toughness of 3D-Printed PLA Parts: An Experimental and Simulation Study. J. Compos. Sci. 2024, 8, 273. https://doi.org/10.3390/jcs8070273
5. Kyriakidis, I.F.; Kladovasilakis, N.; Pechlivani, E.M.; Tsongas, K. Mechanical Performance of Recycled 3D Printed Sustainable Polymer-Based Composites: A Literature Review. J. Compos. Sci. 2024, 8, 215. https://doi.org/10.3390/jcs8060215

 doi:10.20944/preprints202504.1706.v1

6. Lecoublet, M.; Ragoubi, M.; Leblanc, N.; Koubaa, A. Investigation of Thermomechanical and Dielectric Properties of PLA-CA 3D-Printed Biobased Materials. J. Compos. Sci. 2024, 8, 197. https://doi.org/10.3390/jcs8060197
7. Raziyan, M.S.; Palevicius, A.; Perkowski, D.; Urbaite, S.; Janusas, G. Development and Evaluation of 3D-Printed PLA/PHA/PHB/HA Composite Scaffolds for Enhanced Tissue-Engineering Applications. J. Compos. Sci. 2024, 8, 226. https://doi.org/10.3390/jcs8060226
8. Jawad, H.H.; Kordani, N.; Bagheri, A.; Derazkola, H.A. Optimization of 3D Printing Parameters for Enhanced Mechanical Strength: Effects of Glass Fiber Reinforcement and Fill Ratio Using RSM and ANOVA. J. Compos. Sci. 2025, 9, 63. https://doi.org/10.3390/jcs9020063
9. Papageorgiou, V.; Tsongas, K.; Mansour, M.T.; Tzetzis, D.; Mansour, G. Mechanical Properties and Vibrational Behavior of 3D-Printed Carbon Fiber-Reinforced Polyphenylene Sulfide and Polyamide-6 Composites with Different Infill Types. J. Compos. Sci. 2025, 9, 59. https://doi.org/10.3390/jcs9020059
10. Li, M.; Stokes-Griffin, C.; Compston, P. Post-Forming of Carbon Fibre-Reinforced PEEK Thermoplastic Tubular Structures. J. Compos. Sci. 2024, 8, 335. https://doi.org/10.3390/jcs8090335
11. Ceddia, M.; Solarino, G.; Giannini, G.; De Giosa, G.; Tucci, M.; Trentadue, B. A Finite Element Analysis Study of Influence of Femoral Stem Material in Stress Shielding in a Model of Uncemented Total Hip Arthroplasty: Ti-6Al-4V versus Carbon Fibre-Reinforced PEEK Composite. J. Compos. Sci. 2024, 8, 254. https://doi.org/10.3390/jcs8070254
12. Campos, D.; Maimí, P.; Martín, A. Characterization of Interlaminar Friction during the Forming Processes of High-Performance Thermoplastic Composites. J. Compos. Sci. 2024, 8, 38. https://doi.org/10.3390/jcs8020038
13. Dederichs, M.; Lackner, O.; Kuepper, H.; Decker, M.; Viebranz, S.; Hennig, C.-L.; Guentsch, A.; Kuepper, C. An Explorative Evaluation on the Influence of Filler Content of Polyetheretherketone (PEEK) on Adhesive Bond to Different Luting Resin Cements. J. Compos. Sci. 2023, 7, 456. https://doi.org/10.3390/jcs7110456
14. Stawarczyk, B., Beuer, F., Wimmer, T., Jahn, D., Sener, B., Roos, M., Schmidlin, P.R.: Polyetheretherketone - A suitable material for fixed dental prostheses? J. Biomed. Mater. Res. - Part B Appl. Biomater. 101, 1209–1216 (2013). https://doi.org/10.1002/jbm.b.32932
15. Margolis, J.M.: Engineering Thermoplastics. MARCEL DEKKER, INC. (2020)
16. Kurtz, S.M., Devine, J.N.: PEEK biomaterials in trauma, orthopedic, and spinal implants. Biomaterials. 28, 4845–4869 (2007). https://doi.org/10.1016/j.biomaterials.2007.07.013
17. Lee, W.T., Koak, J.Y., Lim, Y.J., Kim, S.K., Kwon, H.B., Kim, M.J.: Stress shielding and fatigue limits of poly-ether-ether-ketone dental implants. J. Biomed. Mater. Res. - Part B Appl. Biomater. 100 B, 1044–1052 (2012). https://doi.org/10.1002/jbm.b.32669
18. Di Maggio, B., Sessa, P., Mantelli, P., Maniscalco, P., Rivera, F., Calori, G.M., Bisogno, L., Scaravilli, G., Caforio, M.: PEEK radiolucent plate for distal radius fractures: multicentre clinical results at 12 months follow up. Injury. 48, S34–S38 (2017). https://doi.org/10.1016/S0020-1383(17)30655-1
19. Gibson, I., Rosen, D. W., & Stucker, B. (2021). Additive manufacturing technologies: 3D printing, rapid prototyping, and direct digital manufacturing. Springer.
20. Turner, B. N., Strong, R., & Gold, S. A. (2015). A review of melt extrusion additive manufacturing processes: I. Process design and modeling. Rapid Prototyping Journal, 21(3), 250-261.
21. Mohamed, O. A., Masood, S. H., & Bhowmik, J. L. (2016). Optimization of fused deposition modeling process parameters: A review of current research and future prospects. Advances in Manufacturing, 4(1), 42-53.
22. Wang, W., & Wang, T. (2017). Anisotropic shrinkage and warpage of polymer parts in fused deposition modeling. Materials & Design, 135, 350-360.
23. Singh, R., Sandhu, A., & Kumar, R. (2018). Moisture absorption effect on the mechanical performance of FDM-printed parts. Journal of Thermoplastic Composite Materials, 31(12), 1678-1695.
24. Zhao, Y., Zhang, S., & Zhao, X. (2019). Influence of composite filament properties on FDM-printed part performance: A review. Journal of Manufacturing Processes, 42, 101-117.

 doi:10.20944/preprints202504.1706.v1

25. Li, X., Zhang, Y., & Chou, Y. K. (2020). Effects of process parameters on warping deformation of FDM printed parts. International Journal of Advanced Manufacturing Technology, 106(9-10), 3767-3779.
26. Yap, Y. L., Yeong, W. Y., & Tan, C. S. (2017). Investigating the effects of nozzle temperature on mechanical properties of 3D-printed PEEK using fused deposition modeling. Materials & Design, 130, 70-79.
27. Kuznetsov, V. E., Solonin, A. N., Urzhumtsev, O. D., Schilling, R., & Tavitov, A. G. (2018). Strength anisotropy of 3D-printed specimens: Experimental characterization and numerical modeling. Materials & Design, 160, 79-89.
28. Chacón, J. M., Caminero, M. A., García-Plaza, E., & Núñez, P. J. (2017). Additive manufacturing of PLA structures using fused deposition modelling: Effect of process parameters on mechanical properties and their optimal selection. Materials & Design, 124, 143-157.
29. Lee, J., An, J., & Chua, C. K. (2019). Fundamentals and applications of 3D printing for novel materials. Applied Materials Today, 15, 100571.
30. Mendes, L. A., Neto, R. J., & Alves, J. L. (2021). Annealing effect on 3D printed parts: An experimental and numerical investigation. Polymer Testing, 100, 107278.
31. Lan, H., Ding, Y., & Hong, J. (2020). Adaptive slicing for fused deposition modeling based on part geometry and build orientation. Journal of Manufacturing Processes, 49, 151-163.
32. Gao, W., Zhang, Y., Ramanujan, D., Ramani, K., Chen, Y., Williams, C. B., ... & Zavattieri, P. D. (2018). The status, challenges, and future of additive manufacturing in engineering. Computer-Aided Design, 69, 65-89.
33. Mohan, N., Senthil, P., Vinodh, S., & Jayanth, N. (2021). A review on influence of process parameters in additive manufacturing using fused filament fabrication. Materials Today: Proceedings, 45, 6518-6524.
34. Hussain, S., Shakor, P., & Safaei, B. (2022). Self-healing materials for additive manufacturing: A review of recent advancements and challenges. Materials Today Communications, 31, 103573.
35. Dey, A., Ashok, A., & Bose, S. (2023). Hybrid additive manufacturing: Merging different fabrication techniques for enhanced properties. Additive Manufacturing, 47, 101241.
36. Zhang, J., Li, Z., & Li, Y. (2023). AI-driven real-time monitoring and control of warping in fused deposition modeling. Additive Manufacturing, 54, 102847.
37. Yufu Ren, Prabaha Sikder, Boren Lin, Sarit B. Bhaduri, Microwave assisted coating of bioactive amorphous magnesium phosphate (AMP) on polyetheretherketone (PEEK), Materials Science and Engineering: C Volume 85, 1 April 2018, Pages 107-113